Article

Time Evolution of Plasmonic Features in Pentagonal Ag Clusters

Nicola Domenis [1,†] (ID), Pablo Grobas Illobre [2] (ID), Margherita Marsili [3] (ID), Mauro Stener [1,*] (ID), Daniele Toffoli [1] (ID) and Emanuele Coccia [1,*] (ID)

1   Dipartimento di Scienze Chimiche e Farmaceutiche, Università degli Studi di Trieste, Via L Giorgieri 1, 34127 Trieste, Italy
2   Scuola Normale Superiore, Piazza dei Cavalieri 7, 56126 Pisa, Italy
3   Dipartimento di Fisica e Astronomia "Augusto Righi", University of Bologna, Viale Berti Pichat 6/2, 40127 Bologna, Italy
*   Correspondence: stener@units.it (M.S.); ecoccia@units.it (E.C.)
†   University of Lyon, Univ Lyon1, Ens de Lyon, CNRS, CRAL UMR5574, F-69230 Saint-Genis-Laval, France.

Abstract: In the present work, we apply recently developed real-time descriptors to study the time evolution of plasmonic features of pentagonal Ag clusters. The method is based on the propagation of the time-dependent Schrödinger equation within a singly excited TDDFT ansatz. We use transition contribution maps (TCMs) and induced density to characterize the optical longitudinal and transverse response of such clusters, when interacting with pulses resonant with the low-energy (around 2–3 eV, A_1) size-dependent or the high-energy (around 4 eV, E_1) size-independent peak. TCMs plots on the analyzed clusters, Ag_{25}^+ and Ag_{43}^+ show off-diagonal peaks consistent with a plasmonic response when a longitudinal pulse resonant at A_1 frequency is applied, and dominant diagonal spots, typical of a molecular transition, when a transverse E_1 pulse is employed. Induced densities confirm this behavior, with a dipole-like charge distribution in the first case. The optical features show a time delay with respect to the evolution of the external pulse, consistent with those found in the literature for real-time TDDFT calculations on metal clusters.

Keywords: time-dependent density functional theory; transition contribution map; induced density

1. Introduction

The optical response of metallic nanostructures to electromagnetic fields has been the subject of intense research activity for many years both at the experimental and theoretical level [1–4]. Such systems are characterized by the simultaneous presence of nearly free electrons confined to a nanometer-size scale and of intense plasmonic excitations of a collective nature. Such intense absorption bands, called Localized Surface Plasmon Resonance (LSPR) are easily tunable [5–7], by playing with size, shape, morphology, and chemical composition when nanoalloys are considered. Such versatility has made them suitable for a wide range of possible scientific and technological applications, ranging from optoelectronics to cancer treatment [1–3,8–11]. From a theoretical point of view, the plasmonic response of large particles (with size beyond 10 nm in each direction) can be predicted by employing variations of the original Mie theory [12] and classical electrodynamics models [13,14], but the extension of these approaches to smaller clusters is questionable due to the emergence of electronic confinement effects, which require quantum mechanical approaches to be properly described. In terms of rigorous information first-principles atomistic approaches, in particular, those based on Time-Dependent Density-Functional-Theory (TDDFT) [15] can make a decisive contribution. Regarding the systems of interest, the optical properties of noble metal nanoclusters with sizes up to some hundreds of atoms were widely studied. For example, tetrahedral Ag nanoclusters in the size range from 10 up to 120 atoms were investigated [16], and it was found that the spectra evolve from

molecular-like to plasmon-like behavior as the size increases, in agreement with classical electrodynamics models. Moreover, the plasmon frequency decreases when the size of the cluster increases [16]. In analogous studies on Au clusters, it was found that the position of the peak in the absorption spectrum was weakly dependent on the shape of the cluster but was essentially related to its size and to the density functional theory (DFT) methodology, i.e., the exchange-correlation (xc-)functional used in the calculations [17]. Similar studies have been performed on Ag clusters of various sizes and shapes (octahedral, truncated octahedral, and icosahedral), confirming the red-shift of the peak position with cluster size and identifying the effect of the cluster shape on the absorption. In particular, a blue-shift with respect to increasing the number of facets is usually predicted by calculations [18]. Moreover, nanorods have also been considered, which are convenient because it is possible to reach a relatively large size in one dimension, thus exploring plasmonic behavior still keeping the cluster nuclearity relatively small [19–22]. A silver nanocage of 60 atoms was considered in Ref. [23], and compared with a hollow nanowire system, finding a similar behavior between the two systems, except that the nanowire gives rise to absorption peaks slightly red-shifted with respect to the nanocage. Larger silver nanocages were considered in [24], while in [25] gold and silver clusters up to M_{309} were considered at the TDDFT level of theory. Some recent applications of linear-response TDDFT considered tetrahedral Ag clusters up to 120 atoms [26], while the plasmonic response of silver, gold, and bimetallic Au–Ag particles of different shapes and sizes were considered in Ref. [27]. In particular, in these latter studies, it is shown how a tight-binding approximation either in the form of TD-DFTB [26] (time-dependent density functional tight binding) or in the linear-response calculation (TD-DFT+TB [27]) can lower by several orders of magnitude the CPU time requirements compared to DFT.

With "molecular plasmonics", two scenarios are usually indicated: i) how the presence of a nanoparticle affects the electronic and optical properties of a molecule close to it [27–36]; ii) collective electronic response to a pulse in subnanometric systems, like metal clusters or molecular aggregates [21,37–44]. In this work, we focus on the latter definition of molecular plasmonics, looking at the time evolution of (collective) optical response of pentagonal silver clusters [19].

The most popular TDDFT approach used to obtain insights into the dynamics of the underlying mechanisms of the plasmonic response of nanoparticles is time propagation in the Kohn–Sham space (RT-RDDFT) [45–51]. Perhaps two of the most promising developments of RT-RDDFT to describe plasmonic systems are when combined with an efficient DFTB scheme [52,53] (RT-TDDFTB) or within orbital-free DFT [54,55]. Alternatively, the time-dependent Schrödinger Equation (TDSE) is propagated in the space of linear-response TDDFT eigenstates [56].

Several works have been dedicated to developing tools to analyze the electron density and dynamics affected by an external perturbation [49,57–66], also to extract possible plasmonic features [46,47,56,67,68].

In this paper, we present results from TDSE propagation [31,69–71] for Ag_{25}^{+} and Ag_{43}^{+} clusters (Figure 1), based on DFT and TDDFT representation of electronic ground and excited states. Electron dynamics are analyzed in terms of possible plasmonic features by means of time-resolved TCMs and induced density [56], with specific attention to longitudinal, i.e., along z, and transverse, i.e., x or y, excitations. The above-mentioned clusters show plasmonic behavior as a function of their length [19], and therefore are good candidates to address plasmonics with a feasible quantum approach.

The article is organized as follows: In Section 2, the theoretical framework is reviewed. Computational details are given in Section 3, results are presented and discussed in Section 4, and conclusions are provided in Section 5.
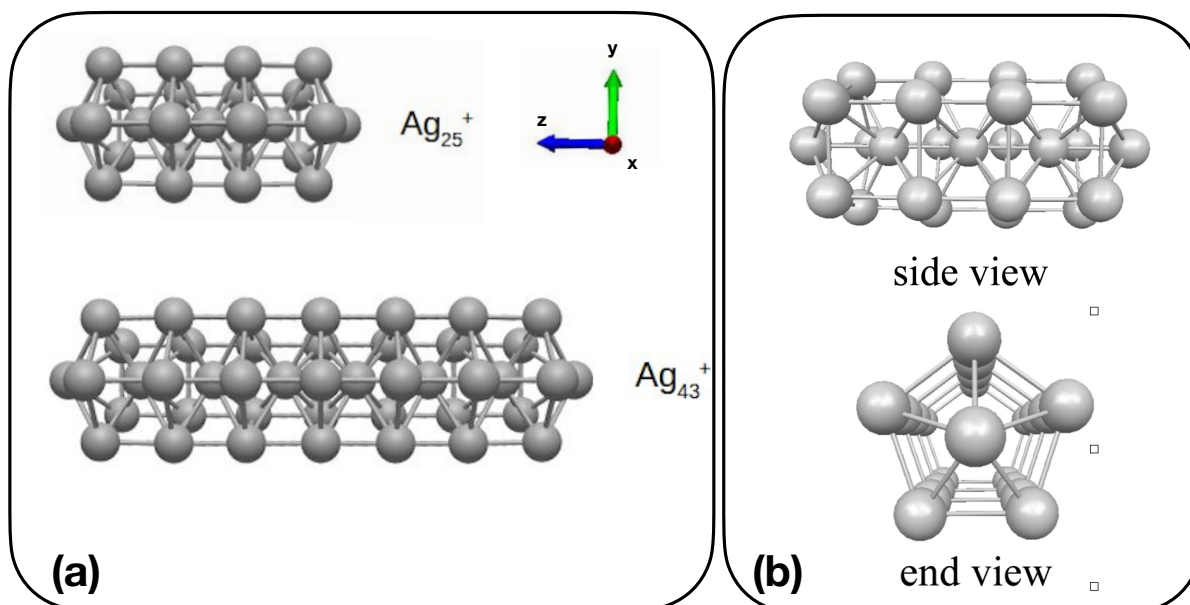
Figure 1. (**a**) Sketch representation of Ag_{25}^+ and Ag_{43}^+; (**b**) side and end view of Ag_{25}^+.

2. Theory

2.1. Real-Time Propagation

TDSE for the electronic dynamics is given by (bra-ket notation and atomic units are used here):

$$i\frac{d}{dt}|\psi(t)\rangle = \hat{H}(t)|\psi(t)\rangle \tag{1}$$

where $|\psi(t)\rangle$ is the time-dependent wavefunction and $\hat{H}(t)$ is the time-dependent Hamiltonian, which includes the field-free Hamiltonian $\hat{H}_{el}$ and the interaction between the system dipole operator $\hat{\boldsymbol{\mu}}$ with the external electromagnetic field $\mathbf{F}(t)$

$$\hat{H}(t) = \hat{H}_{el} - \hat{\boldsymbol{\mu}} \cdot \mathbf{F}(t). \tag{2}$$

We have employed a Gaussian envelope function for the time-dependent external field:

$$\mathbf{F}(t) = \mathbf{F}_{max} \exp\left(-\frac{(t - t_0)^2}{2\sigma^2}\right) \sin(\omega t), \tag{3}$$

where $\mathbf{F}_{max}$ is the field amplitude (the intensity I is equal to $\frac{1}{2}|\mathbf{F}_{max}|^2$), t_0 and σ are the center and the amplitude of the Gaussian, respectively, and ω is the pulse frequency.

In order to simulate a kick pulse, the external electric field $\mathbf{F}(t)$ is given by a narrow Gaussian function.

The electronic time-dependent wavefunction is expanded over the number N_{states} of eigenstates (in our case, the DFT ground state plus the N_{states} TDDFT eigenstates) as

$$|\psi(t)\rangle = \sum_{m=0}^{N_{\text{states}}} C_m(t)|\Phi_m\rangle. \tag{4}$$

In the expansion of Equation (4), $C_m(t)$ are time-dependent expansion coefficients, and $|\Phi_m\rangle$ represents the m-th time-independent TDDFT eigenstate, in the singly excited ansatz [56] of the system, with eigenvalue E_m.

The α-th component of time-dependent dipole moment is computed as follows [56]

$$\mu_\alpha(t) = \sum_{l,m} C_l^*(t) C_m(t) \langle \Phi_l | \hat{\mu}_\alpha | \Phi_m \rangle. \tag{5}$$

The transition dipole $\langle \Phi_l | \hat{\mu}_\alpha | \Phi_m \rangle$ in Equation (5) is obtained from quantum-chemistry calculations [56].

2.2. Electron Dynamics Descriptors

2.2.1. Time-Dependent TCM

TCM, originally defined in the frequency-domain in Ref. [72] is extended to the time domain [56] by

$$\mathrm{TCM}(\epsilon_{occ}, \epsilon_{vir}, t) = 2 \sum_{i,a} \mathrm{Re}\left[\langle \psi(t) | \hat{P}_i^a | \psi(t) \rangle\right] G_{ia}(\epsilon_{occ}, \epsilon_{vir}), \tag{6}$$

where $G_{ia}(\epsilon_{occ}, \epsilon_{vir})$ is a Gaussian function used for convolution, and the projector $\hat{P}_i^a$ extracts the Slater determinant $|\Phi_i^a\rangle$ from the m-th electronic state:

$$|\Phi_m\rangle = \sum_{i,a} d_{i,m}^a |\Phi_i^a\rangle \tag{7}$$

$$\hat{P}_i^a |\Phi_m\rangle = d_{i,m}^a |\Phi_i^a\rangle, \tag{8}$$

with i and a indicating occupied and virtual MOs, respectively.

Using the expansion in Equation (4), and with $\langle \Phi_l | \hat{P}_i^a | \Phi_m \rangle = (d_{i,l}^a)^* d_{i,m}^a$, one obtains

$$\mathrm{TCM}(\epsilon_{occ}, \epsilon_{vir}, t) = 2 \sum_{i,a} \sum_{l,m} \mathrm{Re}\left[C_l^*(t) C_m(t) (d_{i,l}^a)^* d_{i,m}^a\right] G_{ia}(\epsilon_{occ}, \epsilon_{vir}). \tag{9}$$

2.2.2. Time-Dependent Induced Density

The transition density associated with the m-th electronic transition is defined in its diagonal form as

$$\Gamma_m(\mathbf{r}) = \langle \Phi_m | \hat{\rho}(\mathbf{r}, \mathbf{r}) | \Phi_0 \rangle, \tag{10}$$

where $\hat{\rho}(\mathbf{r}, \mathbf{r})$ is the diagonal reduced one-electron density matrix operator, and $|\Phi_0\rangle$ is the DFT ground-state Slater determinant. $\mathbf{r}$ is the collective electronic coordinate.

From the time-dependent expectation value of $\hat{\rho}(\mathbf{r}, \mathbf{r})$ one obtains the time-dependent induced density $\Gamma(\mathbf{r}, \mathbf{r}, t)$ [56]

$$\Gamma(\mathbf{r}, \mathbf{r}, t) = \Gamma_1(\mathbf{r}, \mathbf{r}, t) + \Gamma_2(\mathbf{r}, \mathbf{r}, t) \tag{11}$$

with

$$\Gamma_1(\mathbf{r}, \mathbf{r}, t) = 2 \sum_{m>0} \mathrm{Re}[C_m(t)] \langle \Phi_0 | \hat{\rho}(\mathbf{r}, \mathbf{r}) | \Phi_m \rangle \tag{12}$$

$$= 2 \sum_{m>0} \mathrm{Re}[C_m(t)] \Gamma_m(\mathbf{r}, \mathbf{r}) \tag{13}$$

and

$$\Gamma_2(\mathbf{r}, \mathbf{r}, t) = \sum_{l>0, m>0} C_l^*(t) C_m(t) \langle \Phi_l | \hat{\rho}(\mathbf{r}, \mathbf{r}) | \Phi_m \rangle. \tag{14}$$

$\Gamma_2(\mathbf{r}, \mathbf{r}, t)$ can be neglected since a small intensity, which would lead to a non-appreciable excited-state population, is assumed.

3. Computational Details

Ground-state geometry coordinates of Ag clusters have been taken from Ref. [19]. A +1 charge characterizes the clusters, in order to use a closed-shell formulation of DFT and TDDFT. TDDFT calculations have been performed using AMS suite for codes [73], with a DZ basis set with relativistic corrections and frozen core up to $4p$. Standard Casida approach via Davidson diagonalization has been employed. PBE [74] functional has been chosen.

Real-time propagation has been carried out with WaveT [32,56]. WaveT simulations used as ingredients eigenenergies and transition dipole moments from AMS calculations [56,75]. In order to fill the visible energy range up to 5 eV, we included 750 and 2100 electronic states for Ag_{25}^{+1} and Ag_{43}^{+1}, respectively. 100-fs electron dynamics were simulated, with a time step of 1.21 as. A pulse intensity of 5×10^8 W/cm^2 was employed. FWHM of the resonant pulse from Equation (3) is equal to 15 fs, and that of the kick pulse is equal to 47 as. t_0 was set to 36 fs.

The induced density resulting from a pulse resonant with the frequency of the longitudinal plasmonic peak was represented using an isovalue of 3×10^{-5}. The analog analysis for the transverse plasmonic peak involved an isovalue of 10^{-5} and 3×10^{-5} for the Ag_{25}^+ and Ag_{43}^+ structures, respectively.

4. Results and Discussion

Analysis of plasmonic effects in the electron dynamics of Ag_{25}^+ and Ag_{43}^+ has been performed by focusing on the longitudinal, i.e., z, response of A$_1$ transition and on the transverse, i.e., x or y, response of E$_1$ transition. Because of the symmetry of the clusters (Figure 1), x and y optical responses are equivalent. According to Ref. [19] A$_1$ transition is the "plasmonic" one, which changes with the size of the cluster, while E$_1$ transition is the molecular-like one, which does not show a dependence on the size of the system in terms of frequency. A$_1$ and E$_1$ frequencies have been obtained by inspecting the longitudinal and transverse components of the absorption spectrum, computed using the kick pulse. Figure 2 reports such absorption spectra, for Ag_{25}^+ and Ag_{43}^+. Spectra have been computed as the Fourier transform of the time-dependent dipole moment of Equation (5). From the longitudinal response (left panel of Figure 2) one extracts a maximum frequency, which corresponds to the A$_1$ transition in Ag_{25}^+ and Ag_{43}^+: $\omega = 3.326$ eV for Ag_{25}^+ and $\omega = 2.565$ eV for Ag_{43}^+. E$_1$ frequencies are instead taken from the maxima of the transverse spectra in the right panel of Figure 2: $\omega = 4.078$ eV for Ag_{25}^+ and $\omega = 4.258$ eV for Ag_{43}^+. Arrows in Figure 2 are a guide for the eye.

Let the panel of Figure 3 show the Fourier transform of the z component of the time-dependent dipole moment of Ag_{25}^+ and Ag_{43}^+ (see Equation (5)) when the pulse frequency is resonant with A$_1$ transition. The Fourier transform of the x component of the time-dependent dipole moment of Ag_{25}^+ and Ag_{43}^+ (see Equation (5)) with the pulse frequency equal to the E$_1$ transition is reported in the right panel of Figure 3. In all the cases, a main and narrow peak is located at the transition frequency, as expected. No other transition is involved, only a low signal for the longitudinal spectrum of Ag_{43}^+ is found at around 5.1 eV: these findings suggest that the electron dynamics are dominated by the photoinduced excitation. In other words, the time-resolved features observed by means of TCM and induced density, as shown below, are directly attributable to A$_1$ and E$_1$ transitions.
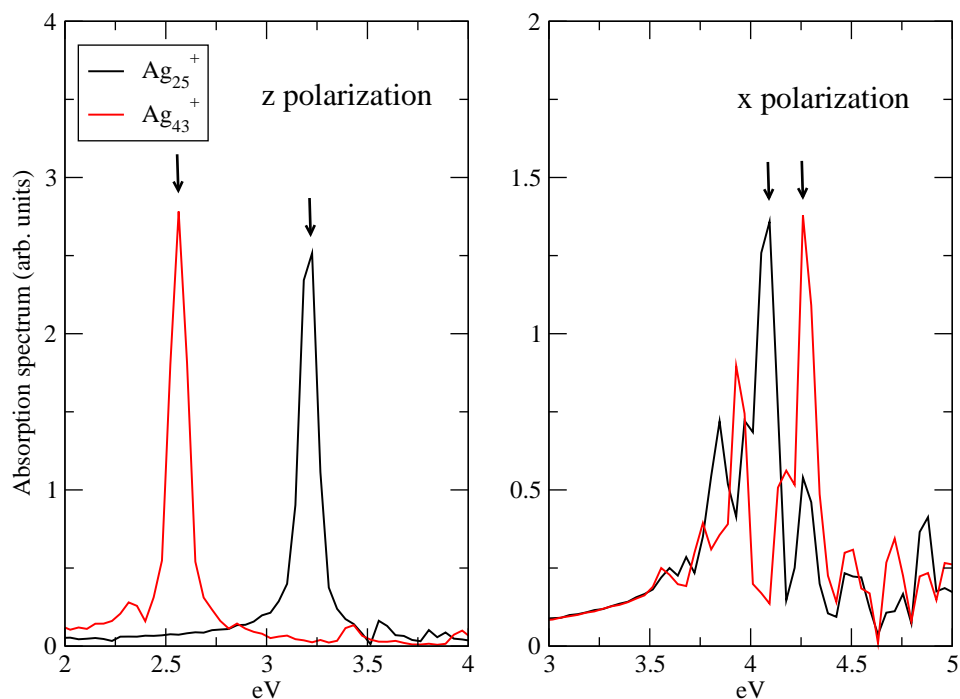
Figure 2. Absorption spectra A_1 (*z* polarization, left panel) and E_1 (*x* polarization, right panel) peaks of Ag_{25}^+ and Ag_{43}^+. Spectra computed using a kick pulse. Spectra normalized to unity. Arrows indicate peaks corresponding to the selected frequencies for the plasmon analysis.
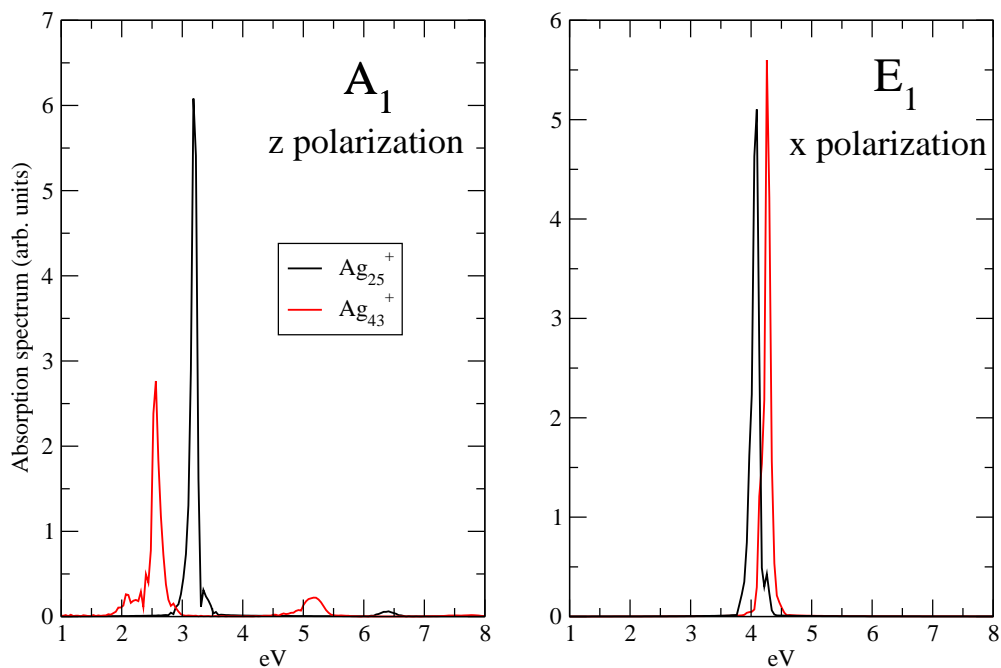
Figure 3. Absorption spectra A_1 (*z* polarization, left panel) and E_1 (*x* polarization, right panel) peaks of Ag_{25}^+ and Ag_{43}^+. Spectra computed using the pulse of Equation (3). Spectra normalized to unity.

Analysis of the electron dynamics of Ag_{25}^+ and Ag_{43}^+ in terms of TCM and induced density has been accomplished considering, for the figures collected below, four time snapshots: 27.6, 36, 44.4, and 60 fs, which correspond to an increasing pulse, pulse maximum, decrease of the pulse, and zero pulse, respectively. These snapshots have been extracted from the whole TDSE dynamics.

Figures 4 and 5 report TCM plots for Ag_{25}^+. TCM is a two-dimensional descriptor able to detect collective features, looking at the single-electron orbital occupation in time: the appearance of off-diagonal spots, with the diagonal corresponding to the pulse frequency, indicates a plasmon-like excitation [39,72,76]. TCM spots are defined with respect to the energies of virtual and occupied MOs, scaled with HOMO energy. When the cluster interacts with a pulse polarized longitudinally with a central frequency corresponding to the A_1 transition, i.e., $\omega = 3.326$ eV, a clear collective response is observed, as reported in Figure 4. Several off-diagonal spots appear, below and above the diagonal. In the first case, the most intense and large ones already appear at 36 fs, and correspond to a one-electron transition from inner MOs 1-2 eV below the HOMO energy to a large portion of virtual MOs. In the second one, a strong spot appears at 44.4 fs, indicating electron promotion from even deeper MOs at around 3.5 eV below the HOMO energy. A rather delayed response of the system seems to occur, since the maximum intensity of the most extended TCM signal (above and below the diagonal) is found after the pulse maximum (top right panel of Figure 4).

(a)

(b)

(c)

(d)
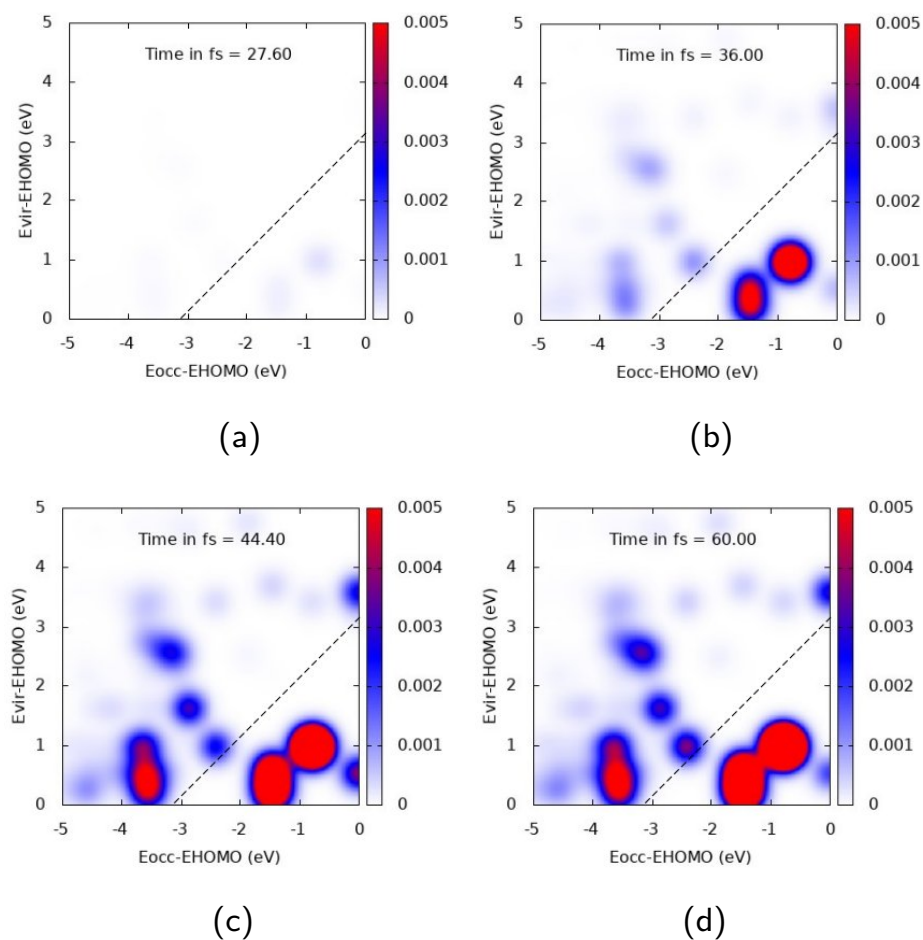
Figure 4. TCM plots for Ag_{25}^+ at the A_1 peak ($\omega = 3.326$ eV), longitudinal z component. (**a**) Snapshot at 27.6 fs; (**b**) Snapshot at 36.0 fs; (**c**) Snapshot at 44.4 fs; (**d**) Snapshot at 60.0 fs.

The nature of the electronic excitation of Ag_{25}^+ dramatically changes when the pulse is polarized transversely to the cluster and resonant with the E_1 transition ($\omega = 4.078$ eV), as shown in Figure 5. In this case, a strong diagonal structure is found, with the highest intensity at 44.4 and 60 fs, giving evidence of the fact that the photoinduced electronic density is dominated by a molecule-like excitation. At 60 fs, the largest spots describe a transition from deep MOs which are 3.5–4 eV below the HOMO to low-energy virtual MOs, and a transition from inner MOs (around 2 eV below the HOMO) to virtual ones 2 eV above the HOMO. TCM spots reach their maximum value well beyond the pulse maximum, confirming that the optical response of the cluster is characterized by a temporal delay with respect to the evolution of the pulse.
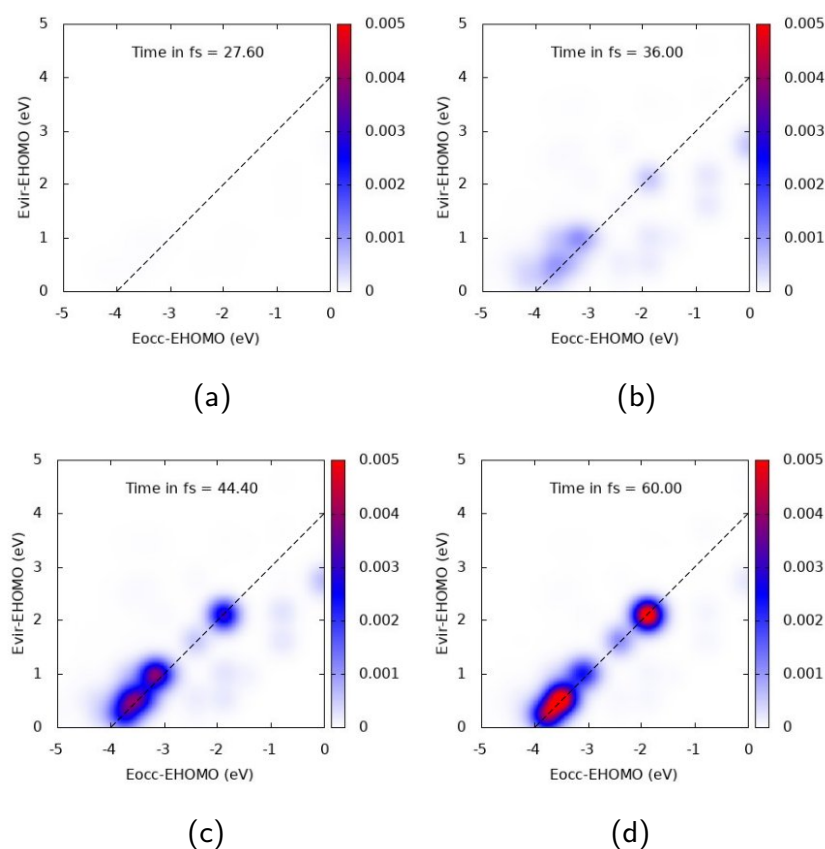
Figure 5. TCM plots for Ag_{25}^+ at the E_1 peak ($\omega = 4.078$ eV), transverse components. (**a**) Snapshot at 27.6 fs; (**b**) Snapshot at 36.0 fs; (**c**) Snapshot at 44.4 fs; (**d**) Snapshot at 60.0 fs.

Similar general comments can be applied to Ag_{43}^+ TCM plots, reported in Figures 6 and 7 for A_1 longitudinal and E_1 transverse responses, respectively. In Figure 6, a strong off-diagonal spot appears at 44.4 fs. The spot describes a one-electron transition from inner occupied MOs to virtual MOs just above the HOMO. At 44.4 and 60 fs an oscillation of the two diagonal spots is also seen, which can be interpreted as a coherent time-dependent superposition of one-electron transitions. Several diagonal peaks instead characterize the TCM in Figure 7, with the most intense one describing an electron promotion from deep MOs (around 4 eV below the HOMO energy) to MOs just above the HOMO energy. The delayed plasmon-like response is also observed for Ag_{43}^+: intensity of off-diagonal peaks obtains its maximum well beyond the pulse maximum, i.e., 36 fs (see Figure 6. Similar behavior is also found for the molecular-like response of Figure 7.

It is worth mentioning that coherent electron dynamics have been carried out, thus no signal decay, due to dephasing or relaxation channels, which can be observed in this framework.
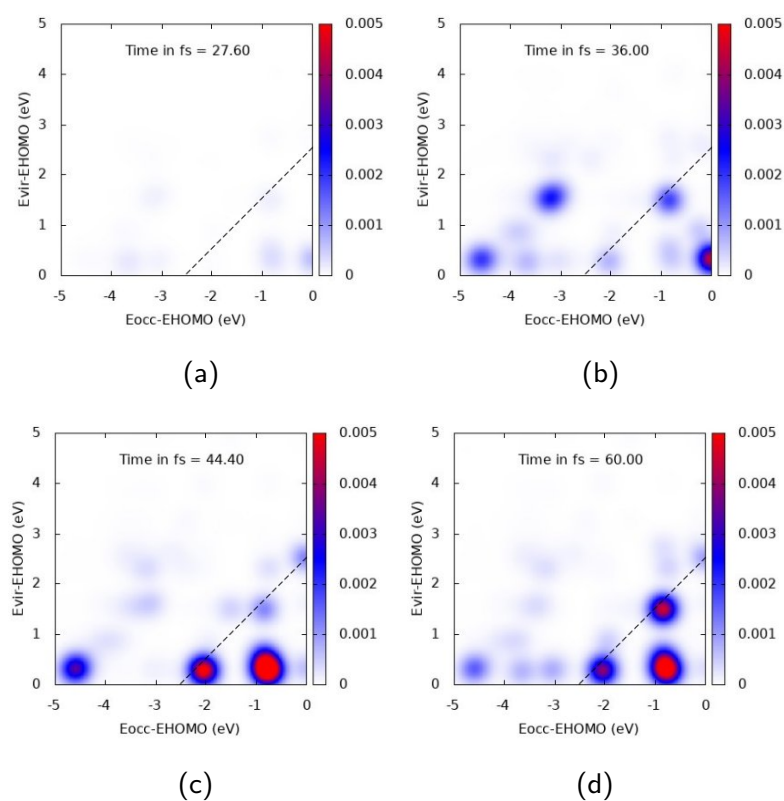
Figure 6. TCM plots for Ag_{43}^+ at the A_1 peak ($\omega = 2.565$ eV), longitudinal z component. (**a**) Snapshot at 27.6 fs; (**b**) Snapshot at 36.0 fs; (**c**) Snapshot at 44.4 fs; (**d**) Snapshot at 60.0 fs.
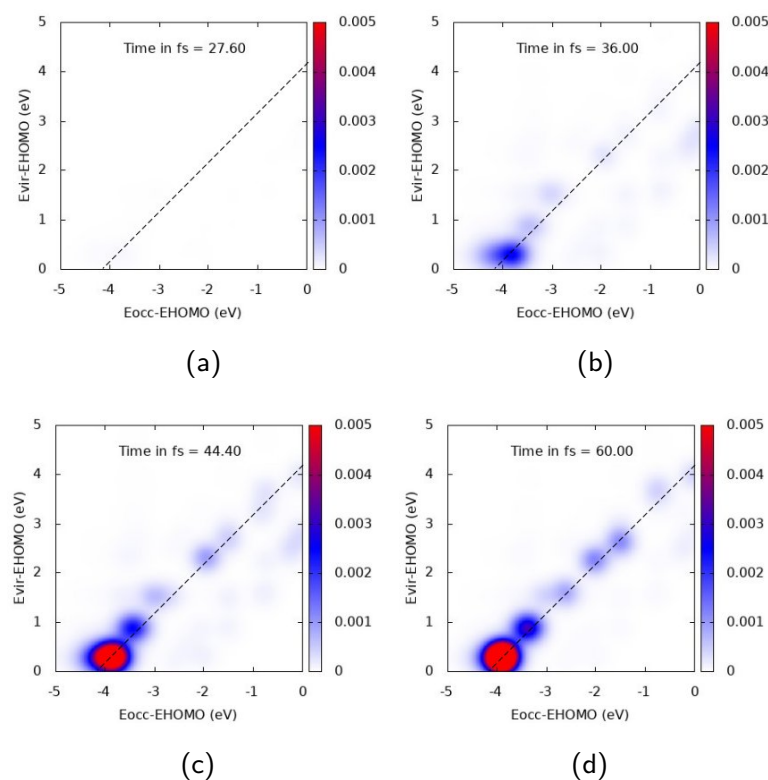
Figure 7. TCM plots for Ag_{43}^+ at the "E_1" peak ($\omega = 4.258$ eV), transverse components. (**a**) Snapshot at 27.6 fs; (**b**) Snapshot at 36.0 fs; (**c**) Snapshot at 44.4 fs; (**d**) Snapshot at 60.0 fs.

Findings given by TCM plots are further supported by the analysis of the time-dependent induced density of Equation (13). Panels (A) and (B) of Figure 8 report $\Gamma_1(\mathbf{r}, \mathbf{r}, t)$ for Ag_{25}^+ interacting with a longitudinal A_1-resonant and transverse E_1 transition, respectively. A dipole-like density is observed in the presence of the A_1-centered pulse, typical of a collective response, whereas a more irregular density is found when the pulse with E_1 central frequency is applied, which corresponds to a standard molecular-like excitation with no plasmonic behavior. Time-dependent induced density for the two pulses has been also computed for Ag_{43}^+, as reported in Figure 9. Similar behavior is found, even though the dipole-like density of Ag_{43}^+ in panel A) of Figure 9 appears more "fragmented" than the Ag_{25}^+. In panel A) of Figures 9 we substantially observe the delayed photoinduced generation of the plasmon. No plasmon decay is observed because coherent dynamics have been performed, as already mentioned.
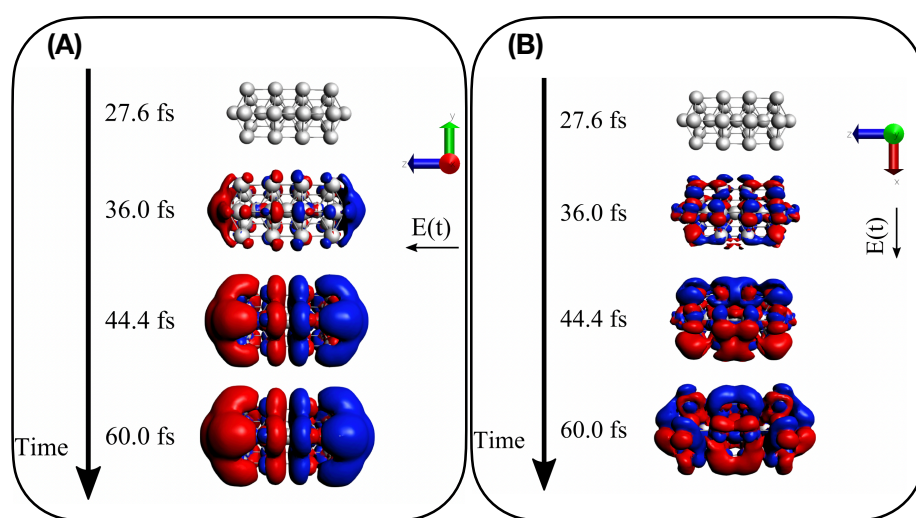
Figure 8. Induced density $\Gamma_1(\mathbf{r}, \mathbf{r}, t)$ as computed in Equation (13) for four different snapshots of electron dynamics of Ag_{25}^+: (**A**) for A_1 longitudinal transition and (**B**) for E_1 transverse transition.
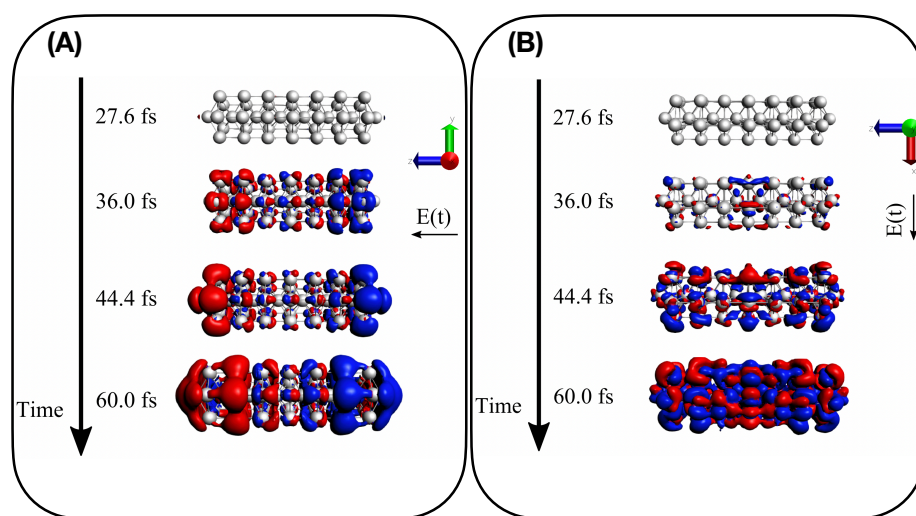
Figure 9. Induced density $\Gamma_1(\mathbf{r}, \mathbf{r}, t)$ as computed in Equation (13) for four different snapshots of electron dynamics of Ag_{43}^+: (**A**) for A_1 longitudinal transition and (**B**) for E_1 transverse transition.

Concerning the time delay of the optical response of the Ag clusters with respect to the pulse, similarly to our findings, a delayed response of the electronic system with respect to the incoming pulse has been reported within the real-time TDDFT (RT-TDDFT) dynamics of an Ag_{55} cluster, for which both dipole moment and charge density difference are at their maxima when the external electric field is already faded out [77]. Interestingly, in the same paper, it was shown how the electron-electron interaction, provided by the TDDFT kernel, is responsible for such delayed features which are absent in an independent particle propagation. This confirms how the electron-electron interaction, at least the part of it that stems from the approximated xc-kernel, is embedded in the present electronic dynamics of Ag_{25}^+ and Ag_{43}^+.

An electronic population dynamics well beyond the pulse duration was also found in RT-TDDFT calculations of water molecules on an Ag/Pt cluster [78] and of a small Ag cluster, for which off-diagonal elements of the density matrix in the space of MOs kept rising [79]. Transition contribution maps of the light-induced RT-TDDFT electronic dynamics of an Ag_{561} cluster, instead, showed only diagonal contributions after the pulse duration [47].

Linear dephasing time experiments found long-lived components, with dephasing times up to $\sim$30 fs for $\sim$90 nm Ag nanoclusters [80]. Indeed future work will be dedicated to the time-evolution of plasmon features in the presence of electron dephasing and relaxation channels, in order to study how the environment, i.e., what is not electronic degrees of freedom of the system, interacts with the excitations [32,81–83].

5. Conclusions

In this work, TDSE was applied to study plasmonic features of pentagonal silver clusters Ag_{25}^+ and Ag_{43}^+.

TDSE was coupled with a linear-response TDDFT description of electronic excited states and with a suite of post-processing tools, able to extract one-electron properties from the time-dependent electronic wavefunction. TDDFT results were obtained using the AMS package, while electronic dynamics were performed via WaveT code.

According to the investigated spectral region, we observed collective features of the electronic excitation or a purely "molecular" response: low-energy transitions are seen to be characterized by off-diagonal peaks in TCM plots, whereas only diagonal spots (i.e., with a single-electron energy difference corresponding to the pulse frequency) are found for high-energy transitions of the absorption spectrum. These features were confirmed by the time-dependent induced densities.

Moreover, an analysis of various snapshots of the time propagation shows that the collective response of the system is generally retarded with respect to the incoming pulse: regardless of the size of the Ag cluster, the largest intensity in the TCM signal is seen beyond the pulse maximum, i.e., 36 fs.

The present results show how the time-resolved theoretical approach is able to capture the physics of metal clusters and, possibly, of composite systems. Future applications of time-resolved TCM and induced density will regard, e.g., the study of the electron dynamics in QM/continuum simulations, as performed for plasmon-enhanced photocatalysis [84–87], and understanding of the interplay between plasmons and quantum coherence [81–83].

Author Contributions: Conceptualization, M.S. and E.C.; methodology, E.C.; software, P.G.I., M.S. D.T. and E.C.; validation, N.D. and P.G.I.; formal analysis, N.D., P.G.I. and E.C.; investigation, N.D., P.G.I. and E.C.; resources, M.S., D.T. and E.C.; data curation, N.D., P.G.I. and E.C.; writing—original draft preparation, M.M., M.S. and E.C.; writing—review and editing, M.M., M.S., D.T. and E.C.; visualization, P.G.I. and E.C.; supervision, E.C.; project administration, E.C.; funding acquisition, M.S., D.T. and E.C. All authors have read and agreed to the published version of the manuscript.

References

1. Ma, Y.Y.; Li, W.Y.; Cho, E.C.; Li, Z.Y.; Yu, T.K.; Zeng, J.; Xie, Z.X.; Xia, Y.N. Au@Ag core-shell nanocubes with finely tuned and well-controlled sizes, shell thicknesses, and optical properties. *ACS Nano* **2010**, *4*, 6725. [CrossRef]
2. Del Fatti, N.; Christofilos, D.; Vallée, F. Optical response of a single gold nanoparticle. *Gold Bull.* **2008**, *41*, 147. [CrossRef]
3. Chen, H.; McMahon, J.M.; Ratner, M.A.; Schatz, G.C. Classical Electrodynamics Coupled to Quantum Mechanics for Calculation of Molecular Optical Properties: a RT-TDDFT/FDTD Approach. *J. Phys. Chem. C* **2010**, *114*, 14384. [CrossRef]
4. Rycenga, M.; Cobley, C.M.; Zeng, J.; Li, W.; Moran, C.H.; Zhang, Q.; Din, Q.; Xia, Y. Controlling the Synthesis and Assembly of Silver Nanostructures for Plasmonic Applications. *Chem. Rev.* **2011**, *111*, 3669. [CrossRef]
5. Yu.; Chang, S.S.; Lee, C.L.; Wang, C.R.C. Gold Nanorods: Electrochemical Synthesis and Optical Properties. *J. Phys. Chem. B* **1997**, *101*, 6661. [CrossRef]
6. Link, S.; Mohamed, M.B.; El-Sayed, M.A. Simulation of the Optical Absorption Spectra of Gold Nanorods as a Function of Their Aspect Ratio and the Effect of the Medium Dielectric Constant. *J. Phys. Chem. B* **1999**, *103*, 3073. [CrossRef]
7. Kelly, K.L.; Coronado, E.; Zhao, L.L.; Schatz, G.C. The Optical Properties of Metal Nanoparticles: The Influence of Size, Shape, and Dielectric Environment. *J. Phys. Chem. B* **2002**, *107*, 668. [CrossRef]
8. Burda, C.; Chen, X.; Narayanan, R.; El-Sayed, M.A. Chemistry and Properties of Nanocrystals of Different Shapes. *Chem. Rev.* **2005**, *105*, 1025. [CrossRef]
9. Marimuthu, A.; Zhang, J.W.; Linic, S. Tuning Selectivity in Propylene Epoxidation by Plasmon Mediated Photo-Switching of Cu Oxidation State. *Science* **2013**, *339*, 1590. [CrossRef]
10. Zhang, J.Z. Biomedical Applications of Shape-Controlled Plasmonic Nanostructures: A Case Study of Hollow Gold Nanospheres for Photothermal Ablation Therapy of Cancer. *J. Phys. Chem. Lett.* **2010**, *1*, 686. [CrossRef]
11. Heo, M.; Cho, H.; Jung, J.W.; Jeong, J.R.; Park, S.; Kim, J.Y. High-performance organic optoelectronic devices enhanced by surface plasmon resonance. *Adv. Mater.* **2011**, *23*, 5689. [CrossRef]
12. Kreibig, K.; Vollmer, M. *Optical Properties of Metal Clusters*; Springer: New York, NY, USA, 1995.
13. Ye, E.; Win, K.Y.; Tan, H.R.; Lin, M.; Teng, C.P.; Mlayah, A.; Han, M.Y. Plasmonic Gold Nanocrosses with Multidirectional Excitation and Strong Photothermal Effect. *J. Am. Chem. Soc.* **2011**, *133*, 8506. [CrossRef]
14. Murray, W.A.; Suckling, J.R.; Barnes, W.L. Overlayers on Silver Nanotriangles: Field Confinement and Spectral Position of Localized Surface Plasmon Resonances. *Nano Lett.* **2006**, *6*, 1772. [CrossRef]
15. Casida, M.E. Time-Dependent Density Functional Response Theory for Molecules. In *Recent Advances in Density Functional Methods*; Chong, D.P., Ed.; World Scientific, Singapore, 1995; Part I, p. 155.
16. Aikens, C.M.; Li, S.; Schatz, G.C. From Discrete Electronic States to Plasmons: TDDFT Optical Absorption Properties of Ag n (n = 10, 20, 35, 56, 84, 120) Tetrahedral Clusters. *J. Phys. Chem. C* **2008**, *112*, 11272. [CrossRef]
17. Durante, N.; Fortunelli, A.; Broyer, M.; Stener, M. Optical Properties of Au Nanoclusters from TD-DFT Calculations. *J. Phys. Chem. C* **2011**, *115*, 6277. [CrossRef]
18. Bae, G.T.; Aikens, C.M. Time-Dependent Density Functional Theory Studies of Optical Properties of Ag Nanoparticles: Octahedra, Truncated Octahedra, and Icosahedra. *J. Phys. Chem. C* **2012**, *116*, 10356. [CrossRef]
19. Johnson, H.E.; Aikens, C.M. Electronic Structure and TDDFT Optical Absorption Spectra of Silver Nanorods. *J. Phys. Chem. A* **2009**, *113*, 4445. [CrossRef]
20. Guidez, E.B.; Aikens, C.M. Diameter dependence of the excitation spectra of silver and gold nanorods. *J. Phys. Chem. C* **2013**, *117*, 12325. [CrossRef]
21. Piccini, G.; Havenith, R.W.A.; Broer, R. Stener, M. Gold nanowires: A time-dependent density functional assessment of plasmonic behavior. *J. Phys. Chem. C* **2013**, *117*, 17196. [CrossRef]
22. ans P. Bonifassi, M.L.; Leszczynski, J.; Ray, P.; Huang, M.; Watts, J. Structure, bonding, and linear optical properties of a series of silver and gold nanorod clusters: DFT/TDDFT studies. *J. Phys. Chem. A* **2010**, *114*, 12701.
23. Mayer, A.; Gonzales, A.L.; Aikens, C.M.; Schatz, G.C. A charge–dipole interaction model for the frequency-dependent polarizability of silver clusters. *Nanotechnology* **2009**, *20*, 195204. [CrossRef]
24. Barcaro, G.; Sementa, L.; Fortunelli, A.; Stener, M. Optical properties of Ag nanoshells from TDDFT calculations. *J. Phys. Chem. C* **2014**, *118*, 12450. [CrossRef]

25. Baseggio, O.; De Vetta, M.; Fronzoni, G.; Stener, M.; Sementa, L.; Fortunelli, A.; Calzolari, A. Photoabsorption of Icosahedral Noble Metal Clusters: An Efficient TDDFT Approach to Large-Scale Systems. *J. Phys. Chem. C* **2016**, *120*, 12773. [CrossRef]

26. Asadi-Aghbolaghi, N.; Rüger, R.; Jamshidi, Z.; Visscher, L. TD-DFT+TB: An Efficient and Fast Approach for Quantum Plasmonic Excitations. *J. Phys. Chem. C* **2020**, *124*, 7946. [CrossRef]

27. D'Agostino, S.; Della Sala, F.; Andreani, L.C. Dipole-excited surface plasmons in metallic nanoparticles: Engineering decay dynamics within the discrete-dipole approximation. *Phys. Rev. B* **2013**, *87*, 205413. [CrossRef]

28. Andreussi, O.; Corni, S.; Mennucci, B.; Tomasi, J. Radiative and nonradiative decay rates of a molecule close to a metal particle of complex shape. *J. Chem. Phys.* **2004**, *121*, 10190. [CrossRef]

29. Caricato, M.; Andreussi, O.; Corni, S. Semiempirical (ZINDO-PCM) Approach to Predict the Radiative and Nonradiative Decay Rates of a Molecule Close to Metal Particles. *J. Phys. Chem. B* **2006**, *110*, 16652.

30. Vukovic, S.; Corni, S.; Mennucci, B. Fluorescence Enhancement of Chromophores Close to Metal Nanoparticles. Optimal Setup Revealed by the Polarizable Continuum Model. *J. Phys. Chem. C* **2009**, *113*, 121. [CrossRef]

31. Mennucci, B.; Corni, S. Multiscale modelling of photoinduced processes in composite systems. *Nat. Rev. Chem.* **2019**, *3*, 315. [CrossRef]

32. Coccia, E.; Fregoni, J.; Guido, C.A.; Marsili, M.; Pipolo, S.; Corni, S. Hybrid theoretical models for molecular nanoplasmonics. *J. Chem. Phys.* **2020**, *200901*, 153. [CrossRef]

33. Gersten, J.; Nitzan, A. Spectroscopic properties of molecules interacting with small dielectric particles. *J. Chem. Phys.* **1981**, *75*, 1139. [CrossRef]

34. Van Duyne, R.P. Molecular plasmonics. *Science* **2004**, *306*, 985. [CrossRef]

35. Novotny, L.; Hecht, B. *Principles of Nano-Optics*; Cambridge University Press: Cambridge, UK, 2012.

36. Wilson, A.J.; Willets, K.A. Molecular Plasmonics. *Annu. Rev. Anal. Chem.* **2016**, *9*, 27. [CrossRef]

37. Bursi, L.; Calzolari, A.; Corni, S.; Molinari, E. Light-induced field enhancement in nanoscale systems from first-principles: the case of polyacenes . *ACS Photonics* **2014**, *1*, 1049. [CrossRef]

38. Adam Lauchner and Andrea E. Schlather and Alejandro Manjavacas and Yao Cui and Michael J. McClain and Grant J. Stec and García de Abajo, F. Javier and Peter Nordlander and Naomi J. Halas. Molecular Plasmonics. *Nano Lett.* **2015**, *15*, 6208.

39. Baseggio, O.; De Vetta, M.; Fronzoni, G.; Stener, M.; Fortunelli, A. A new time-dependent density-functional method for molecular plasmonics: Formalism, implementation, and the Au144(SH)60 case study. *Int. J. Quant. Chem.* **2016**, *116*, 1603. [CrossRef]

40. Zhang, R.; Bursi, L.; Cox, J.D.; Cui, Y.; Krauter, C.M.; Alabastri, A.; Manjavacas, A.; Calzolari, A.; Corni, S.; Molinari, E. How to identify plasmons from the optical response of nanostructures . *ACS Nano* **2017**, *11*, 7321. [CrossRef]

41. D'Agostino, S.; Rinaldi, R.; Cuniberti, G.; Della Sala, F. Density Functional Tight Binding for Quantum Plasmonics. *J. Phys. Chem. C* **2018**, *122*, 19756. [CrossRef]

42. Guerrini, M.; Calzolari, A.; Varsano, D.; Corni, S. Quantifying the Plasmonic Character of Optical Excitations in a Molecular J-Aggregate . *J. Chem. Theory Comput.* **2019**, *15*, 3197. [CrossRef]

43. Müller, M.M.; Kosik, M.; Pelc, M.; Bryant, G.W.; Ayuela, A.; Rockstuhl, C.; Słowik, K. Energy-Based Plasmonicity Index to Characterize Optical Resonances in Nanostructures. *J. Phys. Chem. C* **2020**, *124*, 24331. [CrossRef]

44. James Langford and Xi Xu and Yang Yang. Plasmon Character Index: An Accurate and Efficient Metric for Identifying and Quantifying Plasmons in Molecules. *J. Phys. Chem. Lett.* **2021**, *12*, 9391. [CrossRef]

45. Yabana, K.; Bertsch, G.F. Time-dependent local-density approximation in real time. *Phys. Rev. B* **1996**, *54*, 4484. [CrossRef]

46. Rossi, T.P.; Kuisma, M.; Puska, M.J.; Nieminen, R.M.; Erhart, P. Kohn-Sham Decomposition in Real-Time Time-Dependent Density-Functional Theory: An Efficient Tool for Analyzing Plasmonic Excitations. *J. Chem. Theory Comput.* **2017**, *13*, 4779. [CrossRef]

47. Rossi, T.P.; Erhart, P.; Kuisma, M. Hot-Carrier Generation in Plasmonic Nanoparticles: The Importance of Atomic Structure. *ACS Nano* **2020**, *14*, 9963. [CrossRef]

48. Provorse, M.R.; Isborn, C.M. Electron dynamics with real-time time-dependent density functional theory. *Int. J. Quantum Chem.* **2016**, *739*, 116. [CrossRef]

49. Li, X.; Govind, N.; Isborn, C.; DePrince III, A.E.; Lopata*, K. Real-Time Time-Dependent Electronic Structure Theory. *Chem. Rev.* **2020**, *120*, 9951. [CrossRef]

50. Makkonen, E.; Rossi, T.P.; Larsen, A.H.; Lopez-Acevedo, O.; Rinke, P.; Kuisma, M.; Chen, X. Real-time time-dependent density functional theory implementation of electronic circular dichroism applied to nanoscale metal–organic clusters. *J. Chem. Phys.* **2021**, *154*, 114102. [CrossRef]

51. Sanchez, C.G.; Berdakin, M. Plasmon-Induced Hot Carriers: An Atomistic Perspective of the First Tens of Femtoseconds. *J. Phys. Chem. C* **2022**, *126*, 10015. [CrossRef]

52. Ilawe, N.V.; Oviedo, M.B.; Wong, B.M. Real-Time Quantum Dynamics of Long-Range Electronic Excitation Transfer in Plasmonic Nanoantennas. *J. Chem. Theory Comput.* **2017**, *13*, 3442. [CrossRef]

53. Liu, Z.; Oviedo, M.B.; Wong, B.M.; Aikens, C.M. Plasmon-induced excitation energy transfer in silver nanoparticle dimers: A real-time TDDFTB investigation. *J. Chem. Phys.* **2022**, *156*. [CrossRef]

54. Witt, W.C.; del Rio, B.G.; Dieterich, J.M.; Carter, E.A. Orbital-free density functional theory for materials research. *J. Mater. Res.* **2018**, *33*, 777–795. [CrossRef]

55. Della Sala, F. Orbital-free methods for plasmonics: Linear response. *J. Chem. Phys.* **2022**, *157*, 104101 [CrossRef] [PubMed]

56. Grobas Illobre, P.; Marsili, M.; Corni, S.; Stener, M.; Toffoli, D.; Coccia, E. Time-resolved excited-state analysis of molecular electron dynamics by TDDFT and Bethe-Salpeter equation formalisms. *J. Chem. Theory Comput.* **2021**, *17*, 6314. [CrossRef] [PubMed]

57. Lu, T.; Chen, F. Multiwfn: A multifunctional wavefunction analyzer. *J. Comput. Chem.* **2012**, *33*, 580. [CrossRef] [PubMed]

58. Guido, C.A.; Cortona, P.; Mennucci, B.; Adamo, C. On the Metric of Charge Transfer Molecular Excitations: A Simple Chemical Descriptor. *J. Chem. Theory Comput.* **2013**, *9*, 3118. [CrossRef] [PubMed]

59. Guido, C.A.; Cortona, P.; Adamo, C. Effective electron displacements: A tool for time-dependent density functional theory computational spectroscopy. *J. Chem. Phys.* **2014**, *140*, 104101. [CrossRef]

60. Pohl, V.; Hermann, G.; Tremblay, J.C. An open-source framework for analyzing N-electron dynamics. I. Multideterminantal wave functions. *J. Comput. Chem.* **2017**, *38*, 1515. [CrossRef]

61. Hermann, G.; Pohl, V.; Tremblay, J.C. An open-source framework for analyzing N-electron dynamics. II. Hybrid density functional theory/configuration interaction methodology. *J. Comput. Chem.* **2017**, *38*, 2378. [CrossRef]

62. Lu, T.; Chen, Q. Ultrastrong Regulation Effect of the Electric Field on the All-Carboatomic Ring Cyclo[18]Carbon. *ChemPhysChem* **2020**, *22*, 386. [CrossRef]

63. Liu, Z.; Lu, T.; Chen, Q. Intermolecular interaction characteristics of the all-carboatomic ring, cyclo[18]carbon: Focusing on molecular adsorption and stacking. *Carbon* **2021**, *171*, 514. [CrossRef]

64. Shang, C.; Cao, Y.; Sun, C.; Zhao, H. Theoretical study on an intriguing excited-state proton transfer process induced by weakened intramolecular hydrogen bonds. *Phys. Chem. Chem. Phys.* **2022**, *24*, 8453. [CrossRef]

65. Shang, C.; Sun, C. Substituent effects on photophysical properties of ESIPT-based fluorophores bearing the 4-diethylaminosalicylaldehyde core. *J. Mol. Liq.* **2022**, *367*, 120477. [CrossRef]

66. Zhang, Y.; Shang, C.; Cao, Y.; Sun, C. Quantum mechanics/molecular mechanics studies on the photoprotection mechanisms of three chalcones. *J. Mol. Liq.* **2023**, *372*, 121165. [CrossRef]

67. Kuisma, M.; Sakko, A.; Rossi, T.P.; Larsen, A.H.; Enkovaara, J.; Lehtovaara, L.; Rantala, T.T. Localized surface plasmon resonance in silver nanoparticles: Atomistic first-principles time-dependent density-functional theory calculations. *Phys. Rev. B-Condens. Matter Mater. Phys.* **2015**, *91*, 1–8. [CrossRef]

68. Kumar, P.V.; Rossi, T.P.; Kuisma, M.; Erhart, P.; Norris, D.J. Direct hot-carrier transfer in plasmonic catalysis. *Faraday Discuss.* **2019**, *214*, 189. [CrossRef] [PubMed]

69. Pipolo, S.; Corni, S.; Cammi, R. The cavity electromagnetic field within the polarizable continuum model of solvation: An application to the real-time time dependent density functional theory. *Comput. Theor. Chem.* **2014**, *1040–1041*, 112–119. [CrossRef]

70. Pipolo, S.; Corni, S. Real-Time Description of the Electronic Dynamics for a Molecule Close to a Plasmonic Nanoparticle. *J. Phys. Chem. C* **2016**, *120*, 28774. [CrossRef]

71. Dall'Osto, G.; Gil, G.; Pipolo, S.; Corni, S. Real-time dynamics of plasmonic resonances in nanoparticles described by a boundary element method with generic dielectric function. *J. Chem. Phys.* **2020**, *153*, 184114. [CrossRef]

72. Malola, S.; Lehtovaara, L.; Enkovaara, J.; Häkkinen, H. Birth of the Localized Surface Plasmon Resonance in Monolayer-Protected Gold Nanoclusters. *ACS Nano* **2013**, *7*, 10263. [CrossRef]

73. Rüger, R.; Franchini, M.; Trnka, T.; Yakovlev, A.; van Lenthe, E.; Philipsen, P.; van Vuren, T.; Klumpers, B.; Soini, T. *AMS 2022.1, SCM, Theoretical Chemistry*; Vrije Universiteit: Amsterdam, The Netherlands, 2022.

74. Ernzerhof, M.; Scuseria, G.E. Assessment of the Perdew–Burke–Ernzerhof exchange-correlation functional. *J. Chem. Phys.* **1999**, *110*, 5029–5036. [CrossRef]

75. Monti, M.; Stener, M.; Coccia, E. Electronic circular dichroism from real-time propagation in state space. *J. Chem. Phys.* **2023**, *158*, 084102. [CrossRef]

76. Theivendran, S.; Chang, L.; Mukherjee, A.; Sementa, L.; Stener, M.; Fortunelli, A.; .; Dass, A. Principles of Optical Spectroscopy of Aromatic Alloy Nanomolecules: $Au_{36-x}Ag_x(SPh-tBu)_{24}$. *J. Phys. Chem. C* **2018**, *122*, 4524. [CrossRef]

77. Ma, J.; Wang, Z.; Wang, L.W. Interplay between plasmon and single-particle excitations in a metal nanocluster. *Nat. Commun.* **2015**, *6*, 10107. [CrossRef]

78. Zhang, Y.; Chen, D.; Meng, W.; Li, S.; Meng, S. Plasmon-Induced Water Splitting on Ag-Alloyed Pt Single-Atom Catalysts. *Front. Chem.* **2021**, *9*, 742794. [CrossRef] [PubMed]

79. Kuda-Singappulige, G.U.; Lingerfelt, D.B.; Li, X.; Aikens, C.M. Ultrafast Nonlinear Plasmon Decay Processes in Silver Nanoclusters. *J. Phys. Chem. C* **2020**, *124*, 20477. [CrossRef]

80. Mittal, R.; Glenn, R.; Saytashev, I.; Lozovoy, V.V.; Dantus, M. Femtosecond Nanoplasmonic Dephasing of Individual Silver Nanoparticles and Small Clusters. *J. Phys. Chem. Lett.* **2015**, *6*, 1638. [CrossRef]

81. Coccia, E.; Troiani, F.; Corni, S. Probing quantum coherence in ultrafast molecular processes: An *ab initio* approach to open quantum systems. *J. Chem. Phys.* **2018**, *148*, 204112. [CrossRef]

82. Coccia, E.; Corni, S. Role of coherence in the plasmonic control of molecular absorption. *J. Chem. Phys.* **2019**, *151*, 044703. [CrossRef]

83. Dall'Osto, G.; Coccia, E.; Guido, C.A.; Corni, S. Investigating ultrafast two-pulse experiments on single DNQDI fluorophores: a stochastic quantum approach. *Phys. Chem. Chem. Phys.* **2020**, *22*, 16734. [CrossRef] [PubMed]

84. Vanzan, M.; Marsili, M.; Corni, S. Study of the Rate-Determining Step of Rh Catalyzed CO_2 Reduction: Insight on the Hydrogen Assisted Molecular Dissociation. *Catalysts* **2021**, *11*, 538. [CrossRef]

85. Ezendam, S.; Herran, M.; Nan, L.; Gruber, C.; Kang, Y.; Gröbmeyer, F.; Lin, R.; Gargiulo, J.; Sousa-Castillo, A.; Cortés, E. Hybrid Plasmonic Nanomaterials for Hydrogen Generation and Carbon Dioxide Reduction. *ACS Energy Lett.* **2022**, *7*, 778. [CrossRef] [PubMed]

86. Martirez, J.M.P.; Bao, J.L.; Carter, E.A. First-Principles Insights into Plasmon-Induced Catalysis. *Annu. Rev. Phys. Chem.* **2021**, *72*, 99. [CrossRef] [PubMed]

87. Swearer, D.F.; Zhao, H.; Zhou, L.; Zhang, C.; Robatjazi, H.; Martirez, J.M.P.; Krauter, C.M.; Yazdi, S.; McClain, M.J.; Ringe, E.; et al. Heterometallic antenna-reactor complexes for photocatalysis. *Proc. Natl. Acad. Sci. USA* **2016**, *113*, 8916. [CrossRef] [PubMed]